

Analysis of Tau-pair process in the ILD reference detector model

Taikan Suehara

The University of Tokyo - International Center for Elementary Particle Physics (ICEPP)
7-3-1 Hongo, Bunkyo-ku, Tokyo, 113-0033, Japan

Tau-pair process has been analyzed in the ILD detector model as a benchmark process for LoI. Results of background rejection, forward-backward asymmetry and polarization measurements are obtained with full detector simulation.

1 Goals for LoI

Tau-pair process ($e^+e^- \rightarrow Z^*, \gamma \rightarrow \tau^+\tau^-$) at $\sqrt{s} = 500$ GeV is one of the benchmark processes[1] proposed by Research Director. According to the report, this process is a good sample to examine detector performances of

- tau reconstruction, aspects of particle flow,
- π_0 reconstruction,
- tracking of very close-by tracks.

In this process, tau leptons are highly boosted ($\gamma \sim 140$), thus decay daughters (mainly charged and neutral pions, muons and electrons) are concentrated in a very narrow angle. Reconstruction of π_0 from two photons is especially challenging for the ILC detectors.

Observables for the LoI are cross section, forward-backward asymmetry and polarization of tau leptons. The polarization measurement requires identification of tau decays, including reconstruction of π_0 . Efficiency and purity of event selection cuts should be also a good measure of detector performance.

For physics motivation, tau-pair process is important as a precision measurement of the electroweak theory. For example, measuring cross section and forward-backward asymmetry of tau-pair process very precisely can probe existence of heavy Z' boson.

2 Analysis framework and events

2.1 Event samples

Events of ILD_00 LoI mass production[2] are used for this study. Events reconstructed and listed at DESY by approximately end of February are used in this analysis. 10.3 M SM events generated in SLAC are processed for background estimation with appropriate event weight.

Since the SLAC events have a polarization issues for tau-pair events, tau-pair events generated in DESY are used instead of SLAC events in this analysis. For other modes including tau, SLAC events are used. Whizard 1.51 and TAUOLA[3] are used to generate the DESY events. Statistics of the signal channel is 500 fb^{-1} both for $e_L^- e_R^+$ and $e_R^- e_L^+$ (total 2.3 M events).

Bhabha process (e^+e^- elastic scattering) is an important background for tau-pair analysis. Since the cross section of Bhabha process is too large (~ 17 nb for each polarization in SLAC events), following preselection is applied to the SLAC events before simulation.

- $|\cos\theta|$ of electron or positron must be smaller than 0.96.
- Opening angle between electron and positron must be larger than 165 deg.

After the preselection, the cross section is reduced to 50-90 pb. ~ 1.0 fb $^{-1}$ of preselected Bhabha events are simulated.

Preselection is also applied to $\gamma\gamma \rightarrow \tau\tau$ events with following cuts:

- Opening angle between two taus must be larger than 170 deg.
- Energy sum of two taus is greater than 30 GeV.

The total cross section after the cuts is around 18 pb. Around 100 k events passing preselection are processed.

Integrated luminosity is assumed to be 500 fb $^{-1}$ each for two polarization setups, $e_L^-e_R^+$ and $e_R^-e_L^+$. Assumed polarization ratio is 80% for electron and 30% for positron (i.e. for $e_L^-e_R^+$ setup 90% of electrons are leftly polarized and 65% of positrons are rightly polarized).

2.2 Tau clustering

For tau clustering, an original clustering processor (TaJet) is applied to the output of PandoraPFA. Following is a procedure of the processor.

1. Sort particles in energy order.
2. Select the most energetic charged particle (a tau candidate).
3. Search particles to be associated to the tau candidate. Criteria is:
 - (a) Opening angle to the tau candidate is smaller than 50 mrad., or
 - (b) Opening angle to the tau candidate is not larger than 1 rad. and invariant mass with the tau candidate is less than 2 GeV ($m_\tau = 1.777$ GeV).
4. Combine energy and momentum of the tau candidate and associated particle and treat the combined particle as the new tau candidate.
5. Repeat from 3.
6. After all remaining particles do not meet the criteria, remaining most energetic charged particle is the next tau candidate. (Repeat from 2.)
7. After all charged particles are associated to tau candidates, remaining neutral particles are independently included in the cluster list as neutral fragments.

In the clustering stage, events with > 6 tracks are pre-cut to accelerate clustering since $> 99\%$ of tau decays have ≤ 3 charged particles. Event with only one positive and one negative tau clusters are processed with latter analysis.

Cuts	Tau-pair	Bhabha	$\mu\mu$	$n\ell + n\nu$	$\gamma\gamma \rightarrow \ell\ell$	other $\gamma\gamma, e\gamma$	other
# tracks, # clusters	573180	2.88e+07	590770	1.15e+06	5.58e+08	4.07e+06	1.21e+06
Opening angle > 178 deg.	152865	1.89e+07	157430	7938	6.93e+06	59454	2633
$ \cos\theta < 0.95$	142371	1.39e+07	147571	5020	6.25e+06	57746	610
ee, $\mu\mu$ veto	130383	96482	1606	3225	616265	45645	141
$70 < E_{\text{vis}} < 450$ GeV	125400	5071	635	2953	1641	0	32

(a) e_L^- (80%) e_R^+ (30%)

Cuts	Tau-pair	Bhabha	$\mu\mu$	$n\ell + n\nu$	$\gamma\gamma \rightarrow \ell\ell$	other $\gamma\gamma, e\gamma$	other
# tracks, # clusters	446551	2.68e+07	460874	116198	5.58e+08	46898050	1194395
Opening angle > 178 deg.	127070	1.73e+07	133628	519	6.93e+06	59920	2934
$ \cos\theta < 0.95$	118426	1.23e+07	125113	326	6.25e+06	58987	512
ee, $\mu\mu$ veto	108778	88385	1027	200	616265	46196	107
$70 < E_{\text{vis}} < 450$ GeV	103197	4857	383	183	1641	0	16

(b) e_R^- (80%) e_L^+ (30%)

Table 1: Cut statistics for background suppression. Preselection (See Section 2.1 for details) is applied for Bhabha events before these cuts. Number of events are normalized to 500 fb^{-1} . The same statistics is used for (a) and (b); only event weighting is different.

3 Background suppression

Main background of tau-pair analysis is Bhabha ($e^+e^- \rightarrow e^+e^-$), $WW \rightarrow \ell\nu\ell\nu$ and $\gamma\gamma \rightarrow \tau^+\tau^-$. Since cross sections of Bhabha and two-photon events are huge (about 10^4 and 10^3 larger than signal, respectively), we need tight selection cuts for those background events. Following cuts are applied to signals and all SM background events after the tau clustering.

1. Number of tracks ≤ 6 . Included as a pre-cut in tau clustering processor.
2. Only one positive and one negative tau clusters must exist in the event. (Neutral clusters are allowed.)
3. Opening angle of two tau candidates must be > 178 deg.
This cut efficiently suppresses $WW \rightarrow \ell\nu\ell\nu$ background.
4. ee and $\mu\mu$ events are rejected.

Charged particles depositing $> 90\%$ of their energy in ECAL are identified as electrons, and charged particles depositing $< 70\%$ of their energy (estimated by curvature of their tracks) in ECAL+HCAL are identified as muons. Events with two electrons or two muons are rejected in this cut. This cut is especially for suppressing Bhabha and $e^+e^- \rightarrow \mu^+\mu^-$ events. Signal loss is about 6%.

5. $|\cos\theta| < 0.95$ for both tau clusters.
t-channel Bhabha events are almost completely suppressed by this cut. 20% of signal events are lost.
6. $70 < E_{\text{vis}} < 450$ GeV. E_{vis} does not include energy of neutral clusters.
Lower bound suppresses $\gamma\gamma \rightarrow \tau^+\tau^-$ events, and upper bound suppresses Bhabha events. Signal lost is negligibly small.

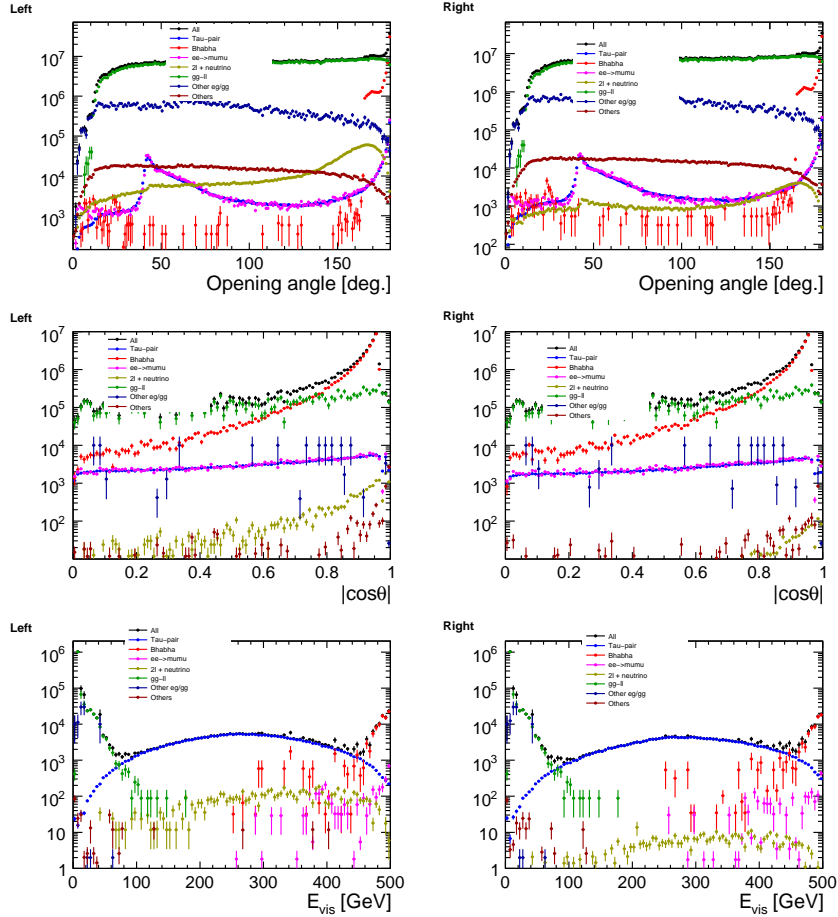


Figure 1: Distribution of cut values. Left column shows $e_L^- e_R^+$ distribution and Right column shows $e_R^- e_L^+$ distribution. Cuts are applied from top, and ee and $\mu\mu$ veto cuts are applied between second and third rows, whose distributions are omitted.

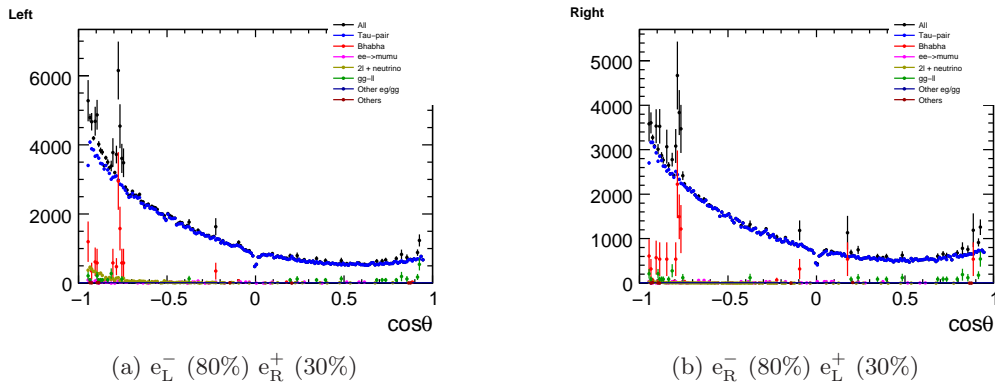


Figure 2: Angular distribution of τ^+ momentum direction. Number of events are normalized to 500 fb^{-1} . Error bars stand for statistical errors in current MC statistics. The same statistics is used for (a) and (b): only event weighting is different.

Table 1 shows the result of these cuts and Figure 1 shows distribution of cut values. Most of the background is effectively cut off by the cuts, $\sim 10\%$ level of the signal. Remaining background is mainly Bhabha, $\gamma\gamma \rightarrow \tau\tau$ and $WW \rightarrow \ell\nu\ell\nu$.

Purity of tau selection is 92.4% in $e_L^- e_R^+$ sample and 93.6% in $e_R^- e_L^+$. The difference is mainly from difference of the cross section between each polarization.

Selection efficiency of tau-pair events is literally low (15.8% in $e_L^- e_R^+$ and 16.3% in $e_R^- e_L^+$). However, the ‘nocut’ number contains radiative events, which have effectively lower \sqrt{s} and should not be used in the analysis. These radiative events are cut by the opening angle selection. The real efficiency varies by the definition of the events. The acceptance of ‘softly-radiated’ tau-pair events is determined by the opening angle cuts. Loosing the cut accepts more events, although $\gamma\gamma \rightarrow \tau\tau$ and $WW \rightarrow \ell\nu\ell\nu$ background significantly increase.

4 Cross section

Cross section can be easily obtained by count-based method since background amount is low. Assuming background subtraction can be performed in the error of statistics, we obtain number of signal event as 125400 ± 368 ($e_L^- e_R^+$) and 103197 ± 332 ($e_R^- e_L^+$), ie. 0.29% and 0.32% statistical error, respectively. The statistical error is dominated by signal statistics, so poor statistics of background events in the current MC sample can only have small effect on these numbers (0.30% and 0.33% statistical error, even if background is doubled). Systematic error can be introduced by polarization error, MC incorrespondance to real detector etc., but it cannot be accurately estimated in this stage of detector development and thus not considered now.

5 Forward-backward asymmetry

Figure 2 shows a result on angular distribution of τ^+ leptons (τ^- events are essentially the same event-by-event since we require opening angle > 178 deg.).

Assuming that background can be subtracted effectively, forward-backward asymmetry is calculated by following formulae.

$$A_{FB} = \frac{N_F - N_B}{N_F + N_B}, \quad (1)$$

$$\sigma A_{FB} = \sqrt{\left(\frac{\partial A_{FB}}{\partial N_F} \sigma N_F\right)^2 + \left(\frac{\partial A_{FB}}{\partial N_B} \sigma N_B\right)^2}, \quad (2)$$

$$\sigma N_F = \sqrt{N_F + N_{FBG}}, \quad \sigma N_B = \sqrt{N_B + N_{BBG}}, \quad (3)$$

where N_B is number of signal events in backward region ($\cos \theta < 0$), N_F is number of signal events in forward region ($\cos \theta > 0$), N_{BBG} is number of background events in the backward region and N_{FBG} is number of background events in the forward region. The formulae can be reduced to

$$\sigma A_{FB} = \frac{2\sqrt{N_B^2(N_F + N_{FBG}) + N_F^2(N_B + N_{BBG})}}{(N_F + N_B)^2}. \quad (4)$$

Result of the calculation is:

$$e_L^- e_R^+ : N_F = 95529, N_B = 29872, N_{FBG} = 9201, N_{BBG} = 1130, A_{FB} = 52.36 \pm 0.25\% (5)$$

$$e_R^- e_L^+ : N_F = 75556, N_B = 27640, N_{FBG} = 5477, N_{BBG} = 1605, A_{FB} = 44.19 \pm 0.28\% (6)$$

Statistical accuracy of A_{FB} is 0.48% and 0.63%, respectively.

6 Decay mode separation

Separating decay modes of tau is essential for the polarization measurement. There are five dominant decay modes of tau, $\tau^+ \rightarrow e^+ \bar{\nu}_e \nu_\tau$ (17.9%), $\tau^+ \rightarrow \mu^+ \bar{\nu}_\mu \nu_\tau$ (17.4%), $\tau^+ \rightarrow \pi^+ \nu_\tau$ (10.9%), $\tau^+ \rightarrow \rho^+ \nu_\tau \rightarrow \pi^+ \pi^0 \nu_\tau$ (25.2%), and $\tau^+ \rightarrow a_1^+ \nu_\tau \rightarrow \pi \pi \pi \nu_\tau$ (9.3% (1-prong) and 9.0% (3-prong)). Other decay modes (10.3%) include Kaons and multi-pions in other resonant modes or continuum.

We utilize a neural network for the decay mode selection. Two separate networks are trained for 1-prong and 3-prong events. 1-prong decay includes $e^+ \bar{\nu}_e \nu_\tau$, $\mu^+ \bar{\nu}_\mu \nu_\tau$, $\pi^+ \nu_\tau$, $\rho^+ \nu_\tau$ and $a_1^+ \nu_\tau$ modes. Input variables of the 1-prong neural net are as follows.

- Two lepton-ID values. Likelihood-based lepton ID software was developed, but due to the known issues of the event production the lepton ID is not properly worked on the mass production sample. As a simpler lepton ID, we use ratio between the energy deposit of the electromagnetic calorimeter (ECAL) and the total deposit energy for the electron ID, and ratio between the calorimeter energy deposit and the track momentum for the muon ID. These two variables are included in the neural network. (Variable (a) and (b).)
- Energy of the charged particle and two kinds of energy sums of the neutral particles. The neutral energy sums contain particles whose ECAL energy deposit is $> 80\%$, and $< 80\%$ of the total energy deposit, respectively. Particles with ECAL energy deposit $< 80\%$ are considered to be hadrons, which contain more spurious particles from a mis-fragmentation of energetic charged particles mainly at HCAL. The energy sums are especially expected to discriminate π mode. (Variable (c), (d) and (e).)

- Number of neutral particles except neutral hadrons. Number of photons is a powerful information to separate ρ (expected number of photons is 2) and a_1 (expected number of photons is 4). (Variable (f).)
- Invariant masses of all reconstructed particles except neutral hadrons and invariant masses of photons. Invariant masses of all reconstructed particles should equal to the masses of intermediate particles, ρ and a_1 . If photons are reconstructed properly, invariant masses of photons are close to that of π_0 . For the photon / hadron separation, above criteria is used again. (Variable (g) and (h).)
- Energy of the third-energetic neutral particle. This variable is also to separate ρ and a_1 . Since ρ can have at most two photons, energy of the third photon should be small even if it exists in the ρ mode. (Variable (i).)

We use two hidden layers, first layer has 18 neurons and second has 9 neurons. The output neurons are likelihood value of $e^+\bar{\nu}_e\nu_\tau$, $\mu^+\bar{\nu}_\mu\nu_\tau$, $\pi^+\nu_\tau$, $\rho^+\nu_\tau$ and $a_1^+\nu_\tau$ modes (5 neurons), which is set to 1(true)/0(false) by the MC information in the training samples.

For the 3-prong events, only a_1 is the discriminating decay mode. Input variables (a), (b), (c), (d), (f), (g), (h) (noted with (a')-(h') in Fig. 4) in the 1-prong selection are also included in the 3-prong selection. There is one additional variable, which is:

- Invariant mass of all charged particles. This should equals to the mass of a_1 if the decay is a_1 mode. (Variable (j').)

We use two hidden layers with 16 and 5 neurons. The only output neuron stands for likelihood value of a_1 mode, set to 1/0 in the training samples as well.

For the training, half of the tau-pair events in the mass production are used. Number of epochs is 1000 for both 1-prong and 3-prong network.

Fig. 3 and 4 shows distributions of the input variables, and Fig. 5 shows distribution of the output neurons. The mode selection is applied based on the values of the output neurons, as follows.

- If one or more of the values of the output neurons exceed 0.5, The neurons which gives the highest output value is used as the selection.
- If no output values exceed 0.5, the event is classified as 'others'.

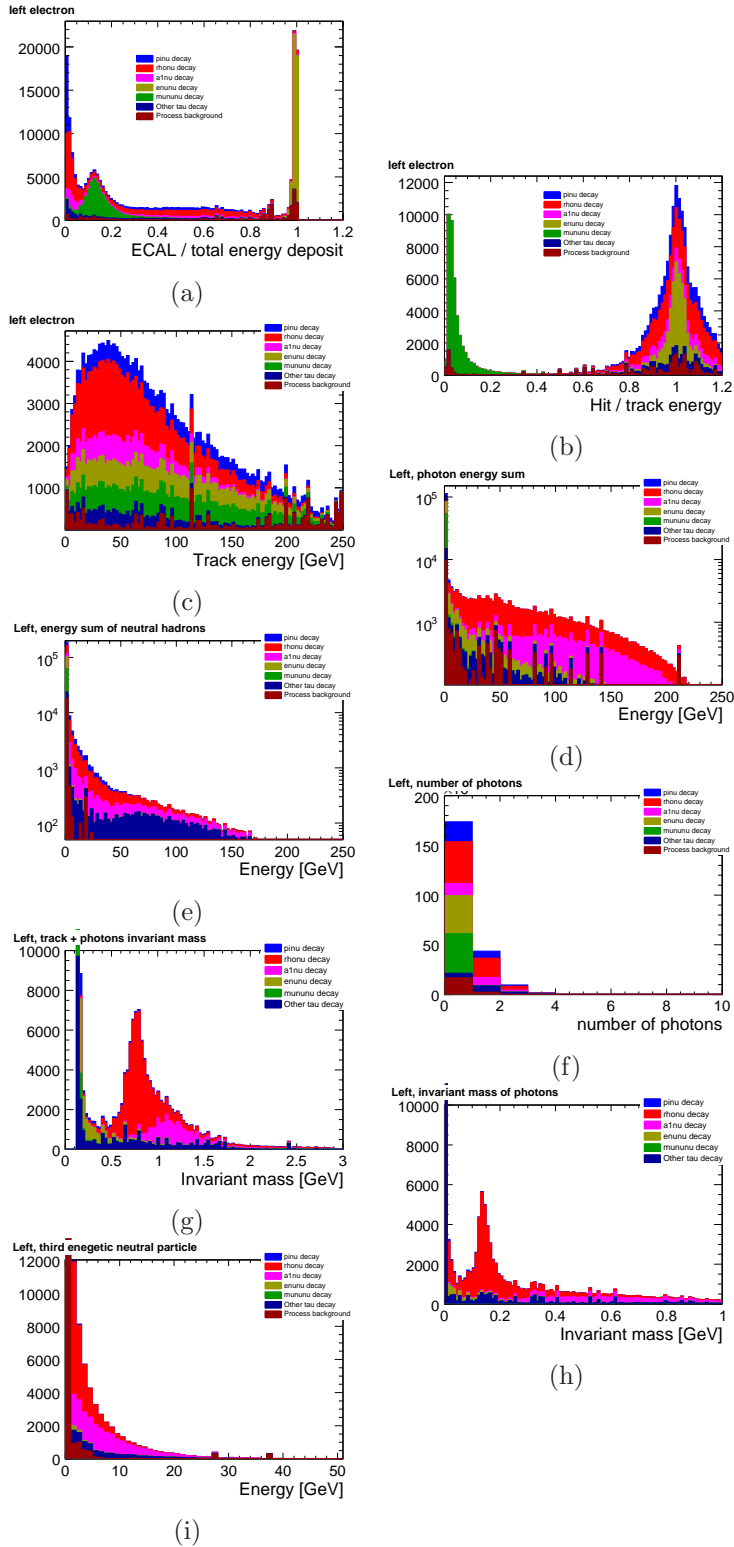
Table 2 shows the obtained efficiency and purity for the mode selection. These values are obtained with the half of the tau-pair events which are not used for the training. $\gtrsim 90\%$ efficiency and purity is obtained for all decay modes except 1-prong a_1 decay.

7 Polarization Measurement

7.1 Optimal Observable

To identify tau polarization, optimal observables[4] are used for $e^+\bar{\nu}_e\nu_\tau$, $\mu^+\bar{\nu}_\mu\nu_\tau$, $\pi^+\nu_\tau$ and $\rho^+\nu_\tau$ decay modes. Decay distribution of all tau decay can be described as the same form,

$$W = \frac{1}{2}(1 + p \cos \theta_h) \quad (7)$$



The 8th general meeting of the ILC physics working group, 1/21, 2009

Figure 3: Distributions of the input variables for the 1-prong neural network. e_L^- (80%) e_R^+ polarization is used for the plots.

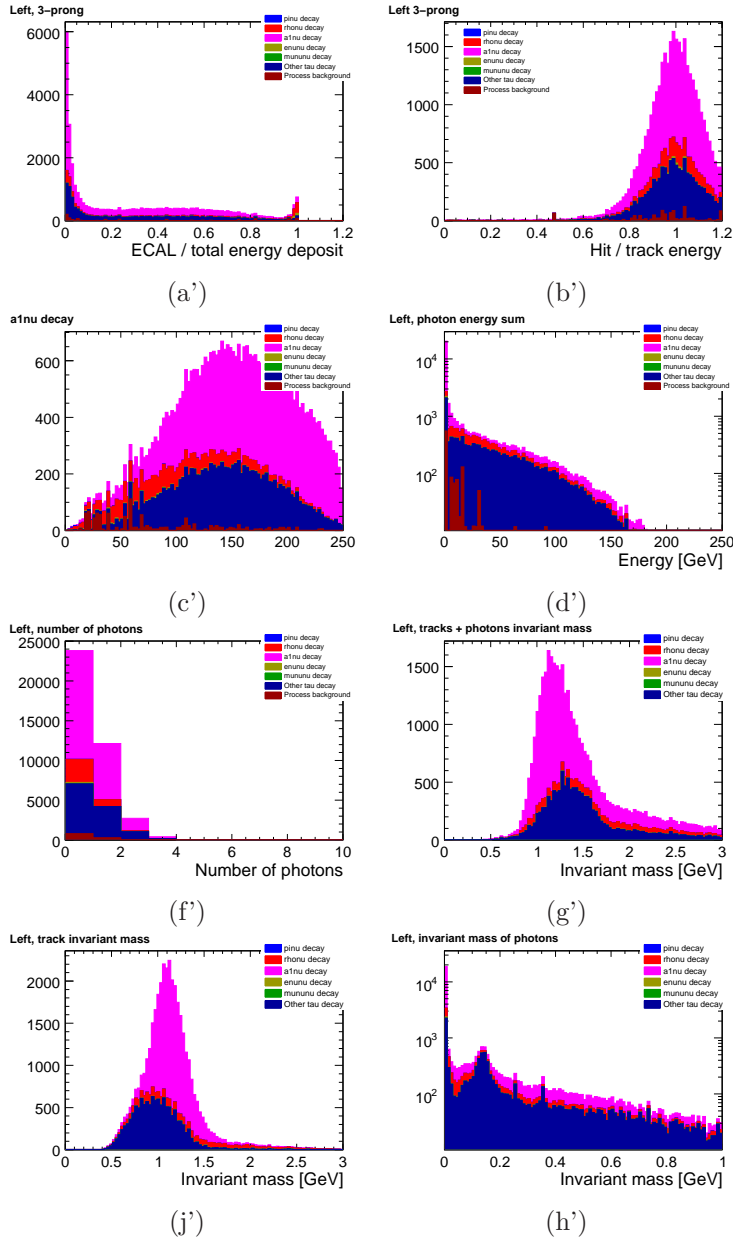


Figure 4: Distributions of the input variables for the 3-prong neural network. e_L^- (80%) e_R^+ polarization is used for the plots.

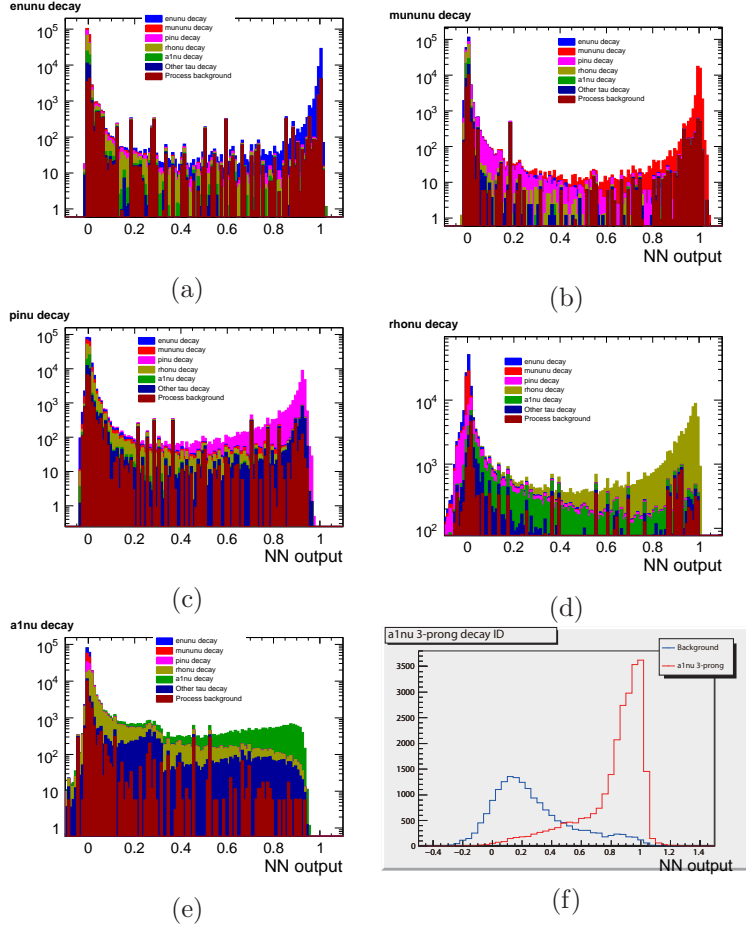


Figure 5: Output variables for the neural net selection. (a)-(e) are the output of the 1-prong neural net for $e^+\bar{\nu}_e\nu_\tau$, $\mu^+\bar{\nu}_\mu\nu_\tau$, $\pi^+\nu_\tau$, $\rho^+\nu_\tau$ and $a_1^+\nu_\tau$ modes, respectively. (f) is the output of the 3-prong neural net for $a_1^+\nu_\tau$ identification. e_L^- (80%) e_R^+ polarization is used for the plots.

Modes	Purity	Efficiency
$e\nu\nu$	98.9%	98.9%
$\mu\nu\nu$	98.8%	99.3%
$\pi\nu$	96.0%	89.5%
$\rho\nu$	91.6%	88.6%
$a_1\nu$ (1-prong)	67.2%	73.4%
$a_1\nu$ (3-prong)	91.1%	88.9%

Table 2: Purity and efficiency of the tau decay mode selection with neural networks. Process background is not included in the purity & efficiency numbers.

where p is polarization of τ (-1 to 1) and θ_h is the opening angle of polarimeter vector \vec{h} with respect to the τ momentum vector. Explicit notation of \vec{h} varies by the decay modes: for pure-leptonic decay, flight direction of antineutrino is \vec{h} and for $\pi^+\nu_\tau$ decay, flight direction of pion is \vec{h} . For the multipion decay, \vec{h} is constructed from the hadronic current.

To reconstruct p from a set of observables, we split W to p -dependent and p -independent components such as

$$W(\vec{\xi}) = f(\vec{\xi}) + pg(\vec{\xi}), \quad (8)$$

and the optimal observable ω is defined as

$$\omega = \frac{g(\vec{\xi})}{f(\vec{\xi})}. \quad (9)$$

By definition, probability density P at ω for the polarization p gives

$$\frac{P(\omega; p) - P(\omega; p = 0)}{P(\omega; p = 0)} = \omega \quad (10)$$

and p can be easily obtained from the ω distribution.

The explicit formula of ω for each decay mode is as follows[5].

1. Pure-leptonic decay:

$$\omega_\ell = \frac{1 + x - 8x^2}{5 + 5x - 4x^2} \quad (11)$$

where x is the lepton energy divided by τ energy (250 GeV in this case). Since the pure-leptonic decay mode has two missing neutrinos, polarization discrimination power is weaker than semi-leptonic decay modes.

2. $\pi^+\nu_\tau$ decay:

$$\omega_\pi = 2x - 1. \quad (12)$$

This mode has maximum polarization discrimination power since \vec{h} can be fully reconstructed.

3. $\rho^+\nu_\tau$ decay: This decay mode has multiple observable particles and thus more complicated formula to describe ω . Tau momentum direction is unobservable in this decay, so it is integrated out in the ω formulation. The explicit formula is:

$$\omega_\rho = \frac{\left(-1 + \frac{m_\tau^2}{Q^2} + 2\left(1 + \frac{m_\tau^2}{Q^2}\right) \frac{3 \cos^2 \psi - 1}{2} \frac{3 \cos^2 \beta - 1}{2}\right) \cos \theta + 3 \sqrt{\frac{m_\tau^2}{Q^2} \frac{3 \cos^2 \beta - 1}{2}} \sin 2\psi \sin \theta}{2 + \frac{m_\tau^2}{Q^2} - 2\left(1 - \frac{m_\tau^2}{Q^2}\right) \frac{3 \cos^2 \psi - 1}{2} \frac{3 \cos^2 \beta - 1}{2}} \quad (13)$$

$$\cos \psi = \frac{x(m_\tau^2 + Q^2) - 2Q^2}{(m_\tau^2 - Q^2)\sqrt{x^2 - 4Q^2/s}} \quad (14)$$

$$x = 2 \frac{E_h}{\sqrt{s}} \quad (15)$$

where E_h is the energy sum of ρ (which equals to the cluster energy), Q^2 is the invariant mass of the visible particles (should equals to $m_\rho = 0.77$ GeV but obtained from the event), \sqrt{s} is the center-of-mass energy (500 GeV), θ is the angle of the ρ flight direction with respect to τ direction in τ -rest frame, and β is the angle of the charged pion flight direction with respect to ρ direction in ρ -rest frame.

7.2 Polarization measurement

Figure 6 shows the ω distribution for each decay mode passing the neural net selection. For the leptonic mode, most of the events are concentrated on the $\omega \sim 0$ region, reflecting to the weak discrimination power. For the $\pi^+\nu_\tau$ and $\rho^+\nu_\tau$ modes, ω distribution is broadly distributed and large difference between left and right polarization can be seen.

Polarization p can be obtained by following procedure.

1. Mode and process background is eliminated from each bin of the ω histograms and statistical error of background remains included in the error of each bin.
2. Histograms from all decay modes are summed into one histogram.
3. The histogram with polarizing sample (polarization p) is divided by non-polarizing sample after normalizing both histograms.
4. Perform linear fit passing (0,1) to the divided histogram (one parameter fit). Obtained slope stands for p .

Figure 7 shows the combined ω distribution and Figure 8 shows the linear fits to obtain p value. Obtained p is $-63.82 \pm 0.66\%$ ($e_L^- e_R^+$, 80% and 30%) and $50.83 \pm 0.79\%$ ($e_R^- e_L^+$, 80% and 30%).

8 Summary

Tau-pair process has been analysed in the ILD_00 detector model. After the tau selection cuts, statistical error of cross section measurement is 0.29% ($e_L^- e_R^+$, with 80% and 30% polarization, respectively) and 0.32% ($e_R^- e_L^+$). Process background can be suppressed to around 10% of signal events. Forward-backward asymmetry can be determined with 0.48% and 0.63% statistical error.

Polarization measurement needs separation of decay modes. The neural net selection gives $> 91\%$ efficiency and $> 88\%$ purity of mode selection for all major decay modes except $a_1\nu$ 1 prong mode. Polarization analysis of $e^+\bar{\nu}_e\nu_\tau$, $\mu^+\bar{\nu}_\mu\nu_\tau$, $\pi^+\nu_\tau$ and $\rho^+\nu_\tau$ decay mode is performed using the optimal observable method, and it results in $P(\tau) = -63.82 \pm 0.66\%$ ($e_L^- e_R^+$) and $P(\tau) = 50.83 \pm 0.79\%$ ($e_L^- e_R^+$).

The $a_1\nu_\tau$ mode is not included in the current polarization measurement. For the 3-prong a_1 decay, τ direction can be reconstructed from the vertex information and it can improve the analysis power to the same level as $\pi^+\nu_\tau$ mode. However, since the branching ratio of 3-prong a_1 decay is only about 9%, the expected improvement with 3-prong a_1 decay is about 20%.

References

- [1] The WWOC Software panel: T. Behnke, N. Graf and A. Miyamoto, ILC-MEMO-2008-001.
- [2] http://ilcsoft/desy.de/portal/data_samples
- [3] S. Jadach, Z. Ws, R. Decker, JH. Kuehn, Comp. Phys. Comm. **76** 361 (1993).
- [4] M. Davier, L. DufLOT, F. Le Diberder and A. Rouge, Phys. Lett. B. **306** 411 (1993).
- [5] L. DufLOT, PhD. thesis, Paris-Sud 11 University in Orsay, 1993.

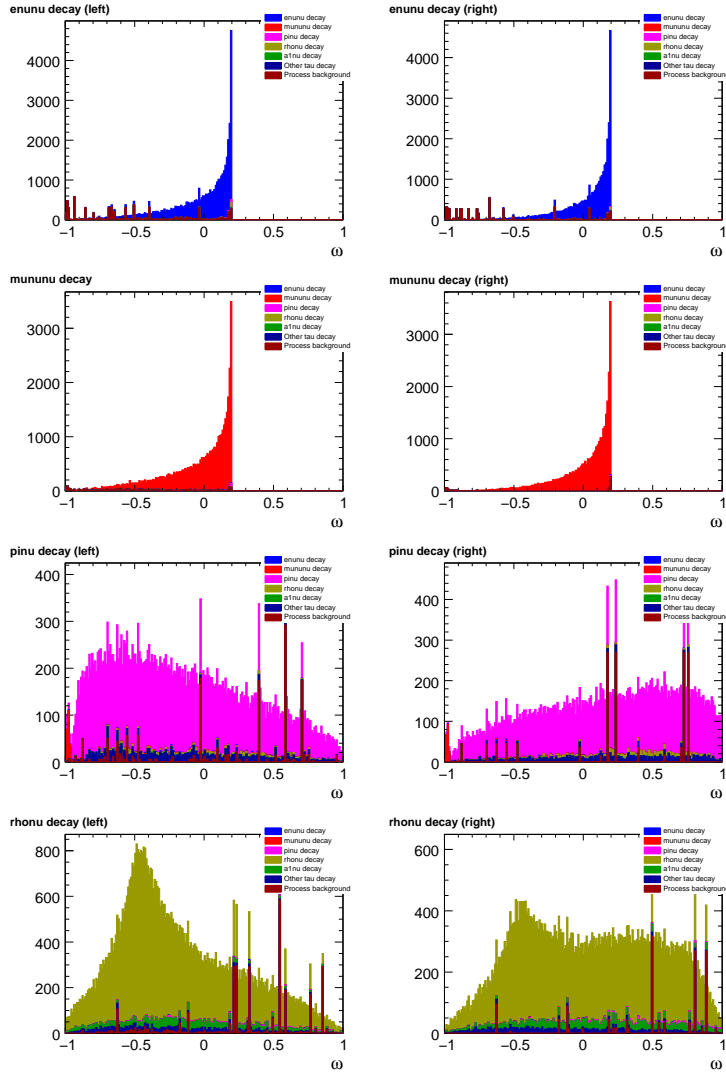


Figure 6: Distribution of the optimal observable for each decay mode. The left column shows distribution of e_L^- (80%) e_R^+ (30%) events, and the right column shows distribution of e_R^- (80%) e_L^+ (30%) events.

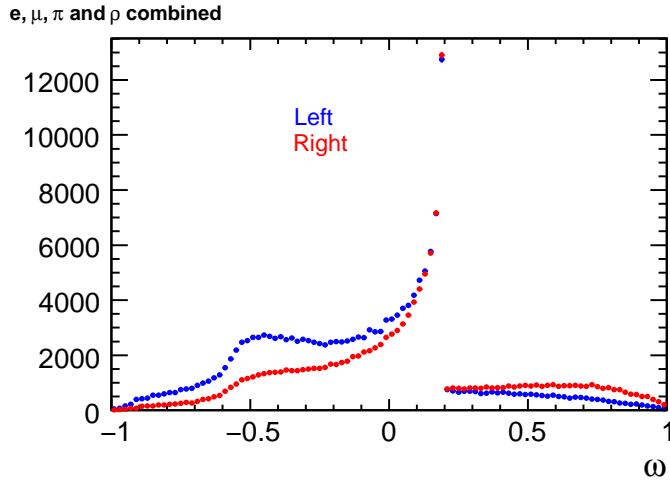


Figure 7: Distribution of the optimal observable after summing up all decay modes.

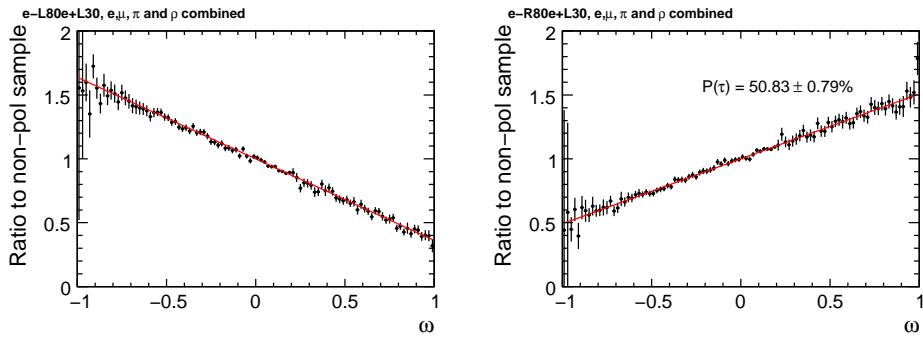


Figure 8: Ratio of the polarizing sample to the non-polarizing sample. Linear fit is applied to obtain p value.